The 8th European Congress on Computational Methods in Applied Sciences and Engineering
ECCOMAS Congress 2022
5-–9 June 2022, Oslo, Norway

NUMERICAL INVESTIGATION OF OLEO-PNEUMATIC SHOCK ABSORBER: A MULTI-FIDELITY APPROACH

Ahmed A. Sheikh Al-Shabab[1], Bojan Grenko[1], Dimitrios Vitlaris[1], Panagiotis Tsoutsanis[1], Antonis F. Antoniadis[1] and Martin Skote[1]

[1] School of Aerospace, Transport and Manufacturing, Cranfield University,
College Road, Cranfield, Bedfordshire, MK43 0AL, UK
Corresponding Author: A.A.Sheikh-Al-Shabab@Cranfield.ac.uk

Key words: Shock Absorbers, Turbulence, Multiphase, Multifidelity

Abstract. A representative shock absorber geometry is developed based on the general guidelines available in the literature, and it is validated against experimental measurements from a drop test. Simulations are conducted using a multi-fidelity approach ranging from unsteady scale resolving three-dimensional simulations to dynamic system models. High fidelity simulations provide a detailed insight into the flow physics inside the shock absorber, as well as help calibrate and validate lower fidelity methods, under conditions for which no experimental measurements are available to achieve that purpose. On the other hand, lower fidelity methods are used to efficiently scan the design space and test the dependency of the shock absorber performance on the various design parameters, in addition to identifying parameter combinations that would be of interest to investigate using a high-fidelity approach.

1 INTRODUCTION

The internal flow dynamics of Oleo-pneumatic shock absorbers remains a challenging area of ongoing research. The multiphysics nature of the problem makes it difficult to identify the dominant features of the flow field and the conditions under which important phenomena, such as cavitation, are likely to become significant in a given design. Hence, it is desired to develop a framework that allows the performance of shock absorbers to be explored in a systematic manner.

A main difficulty in the investigation of oleo-pneumatic shock absorbers is that there aren't any widely researched standard geometries with known properties, such as, for example, the NACA-series in the case of airfoils. Therefore, a baseline geometry was generated by using the available information from the drop down test used for validation, while the missing parameters were estimated based on the general guidelines and sizing data available in the literature.

The study of Milwitzky and Cook [6] is of particular interest in the present work as it has been used extensively for validation purposes across the different fidelity levels. It has the advantage of providing a comprehensive development of a dynamic system model of landing gear shock absorbers, including tire forces, inclination effects, friction forces and ground forces. It also provides drop test experimental measurement validation data using a small military trainer aircraft, with the shock absorber geometry given to sufficient detail so that, together with the general guidelines of Curry [2], it is possible to reproduce the geometry for high-fidelity

Published by ECCOMAS. This is the Author Accepted Manuscript issued with: Creative Commons Attribution Non-Commercial License (CC:BY:NC:SA 4.0).
The final published version (version of record) is available online at DOI:10.23967/eccomas.2022.201. Please refer to any applicable publisher terms of use.

simulations. Given all the above, while this study is relatively old, it remains one of the best comprehensive studies of shock absorber modelling and validation. It should be noted that while the aforementioned study has been around for decades, there is a gap in the literature regarding the simulation of internal dynamics that govern the shock absorber system, hence there is an interesting aspect of novelty to the work conducted on the medium and high-fidelity simulation of this case.

2 METHODOLOGY AND NUMERICAL METHODS

The prediction of shock absorber performance requires accounting for a range of physical phenomena that are expensive to compute directly using fully resolved three-dimensional simulations. The main dominant features include the multiphase interaction between the hydraulic oil and gas inside the shock absorber, see Fig. 1a in addition to the turbulent shear flow through the orifice. The multiphase interaction has an influence on the variation of working fluid properties as the stroke progresses, while the developing turbulent flow downstream of the orifice is central to the energy absorption within the shock absorber.

It is possible to conduct an integrated multi-physics shock absorber simulation, that accounts for most of the flow physics in a single simulation. However, it is more efficient (and computationally stable) to adopt a modular approach that uses specialised tools concentrating on each of the flow physics in turn, particularly when a large number of simulations are planned to explore the design space. In this modular approach, understanding the coupling between the various aspects of flow physics requires careful consideration, and potentially a few integrated fully coupled multi-physics simulations. Nevertheless, the benefit of taking advantage of the most efficient and well developed tool in each area is attractive. The chosen numerical solvers have been validated on model problems that are representative of the flow physics of interest [10].

Similarly, adopting a multi-fidelity approach increases the efficiency of design space exploration by using the expensive high-fidelity models to provide basic flow physics understanding and to calibrate lower fidelity models in different flow regimes.

2.1 MULTIPHASE SIMULATION

Multiphase simulation cases are conducted with ANSYS Fluent 2019 R2. The cases are set up as 2D half sections with an axisymmetric boundary condition. A Pressure based (incompressible) solver is used with the unsteady RANS $k-\omega$ SST turbulence model. Ideal gas law is used to account for gas compressibility in combination with the selected incompressible solver. The multiphase modelling method is an explicit formulation of the volume of fluid scheme with sharp interface modelling. The domain is filled with two phases: hydraulic oil *MIL-H-5606*, and air. The boundary conditions surrounding the domain are all walls apart from axis on the shock absorber symmetry line, and a time dependent velocity inlet instead of the bottom wall. The velocity inlet imitates compression and expansion with positive and negative velocities, so that a moving mesh can be avoided, allowing higher computational efficiency and more flexible meshing options. Pressure and velocity are coupled with the Coupled scheme. The spatial discretization schemes are: PRESTO (PREssure STaggering Option) scheme for pressure, modified HRIC for volume fraction, and second order upwind for the rest of the flow variables. A dual-time step-

ping approach is used with a maximum of 40 sub-iterations per physical time step. Variable time stepping method is applied with a CFL number constraint of 0.3, and a minimum allowed physical time step of $1e-8$ seconds.

2.2 TURBULENT SHEAR LAYER SIMULATION

OpenFoam (v2006) [12, 5] was used to conduct single phase time-dependent scale resolving turbulent shear layer simulations. OpenFoam uses an unstructured finite volume approach to simulate fluid flow, which facilitates the handling of complex geometries that are expected in industrial type applications, as in the case of the shock absorbers investigated here. Field properties are stored at the centroid of each cell and then calculated at each cell surface "face" by interpolating the values at the centroids of the two cells sharing that face. Conservation laws are then applied based on theses face values, in accordance with the chosen discretization scheme.

The PIMPLE algorithm [3] is selected in the present simulations, as it provides good stability and convergence control options. PIMPLE utilises an outer loop based on the PISO algorithm [4] to capture the field development in time, while an inner loop based on the SIMPLE algorithm [8] solves each field instance as a steady problem. The interpolation method used in the present study is a second order linear interpolation, which is a standard choice in many finite volume solvers. The convective term is discretized using a second order limited linear scheme, which provides a balance between accuracy and stability through limiting the nonlinear term. While the diffusive term is discretized using a second order linear scheme and temporal integration is conducted using a second order backward difference method, with an adjustable time step to insure that the CFL number remain below 1.0 during the simulation.

After the discretization process, the resulting linear system for the pressure field is solved for using a Preconditioned Conjugate Gradient (PCG) method, while the velocity field system is found using a Preconditioned Bi-Conjugate Gradient method (PBiCG). An adjustable time step is used to insure that the Courant–Friedrich–Lewy (CFL) number remains below 1.0 throughout the simulation, to aid in achieving a balance between efficiency and stability during these simulations. The WALE subgrid scale model [7] is used to model the eddy viscosity of the subgrid scales in the Large Eddy Simulation, (LES) framework. The flow field is allowed to develop by allowing multiple through-flows across the entire domain, then time averaging is conducted until statistical convergence is reached for all turbulent properties of interest.

3 COMPUTATIONAL SETUP

The baseline orifice geometry, illustrated in Fig. 1, has an orifice with semi-circular lips. The rounded outer (upstream) edge of the orifice helps avoid any boundary layer separation on the orifice's inner surface, while the accelerating flow under the influence of the favourable pressure gradient through the orifice allows relatively strong flow turning in the flow direction so that the flow can be tangential to the axial (streamwise) direction at the orifice exit. A three dimensional simulation is conducted on a simplified geometry of the shock absorber that focuses on the orifice nearfield region and the developing shear layer in its vicinity.

Grids of varying resolution were generated and tested to establish grid independence and

optimise the setup, where possible. The resolution in the shear layer region was tested using a preliminary simulation on a grid with 185,000 nodes. An analysis was conducted to check the required resolution in the main simulation, including looking at the estimated mixing layer thickness near the orifice tip to determine the grid resolution required there. The boundary conditions are illustrated in Fig. 1b, while further information about the case is provided in Table 1.

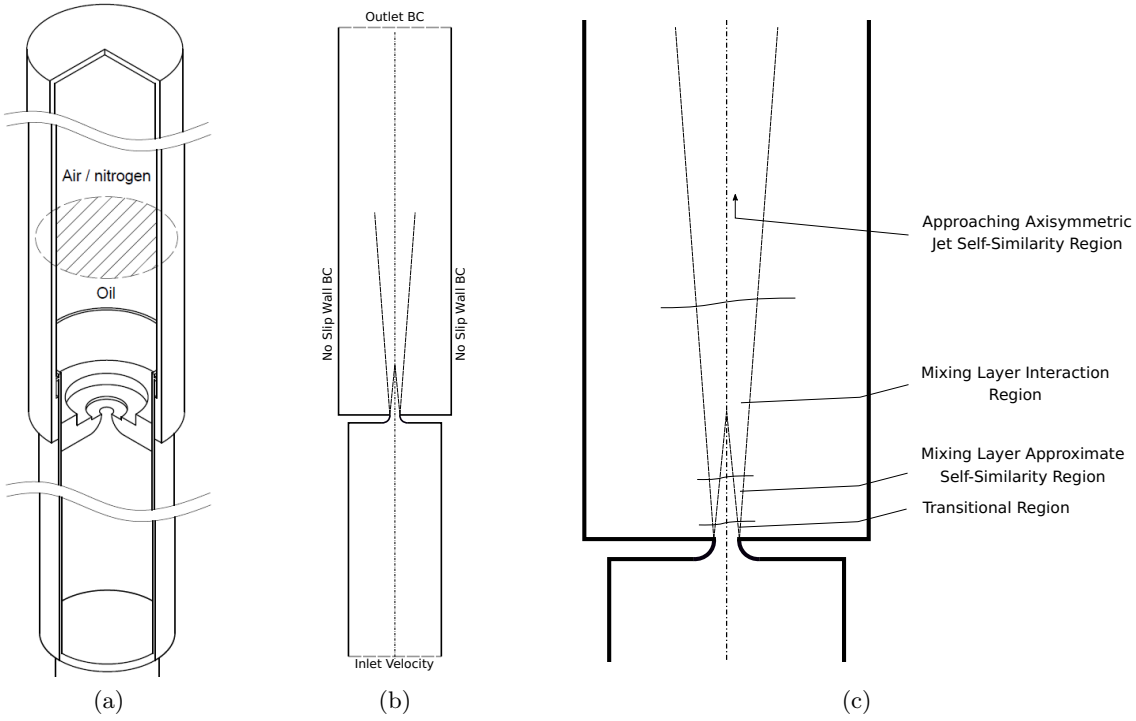


Figure 1: Shock absorber geometry and some setup details (**a**) Schematic view of the simplified shock absorber geometry; (**b**) The computational domain with the applied boundary conditions; (**c**) Axisymmetric shear layer development regions, following Bradshaw et al. [1].

Simulation Parameter	**Setting**
Working Fluid type	Hydraulic Oil (AN-VV-O-366B)
Hydraulic Oil Density, ρ_h (kg/m^3)	869
Hydraulic Oil Kinematic Viscosity, ν_h (m^2/s)	1.35×10^{-5}
Time step	$\approx 8 \times 10^{-7}$
Orifice Diameter, m	8.128×10^{-3}
Inlet Velocity, m/s	1.0
Total Grid Nodes	1.8×10^6

Table 1: Scale resolving 3D axisymmetric free shear layer simulation

The inlet boundary condition is taken to be a constant vertical flow through the shock absorber $V = 1.0$ m/s as a representative figure of an approximately time-averaged value over the stroke period from the Milwitzky and Cook [6] drop test. The stroke shape and value, corresponding to the drop test, can be seen in Fig. 2, where this figure was obtained using a

dynamic system model simulation of the drop test following the analysis in Milwitzky and Cook [6]. The initial delay in the response of the shock absorber, the flat region at time = 0.0 s, is due to the force required to deflect the tire and other internal effects (e.g., the gas pressure force), which leads to the shock absorber behaving as a rigid body during the early stages of impact; however, this is quickly overcome by the impact resulting in the subsequent stroke profile.

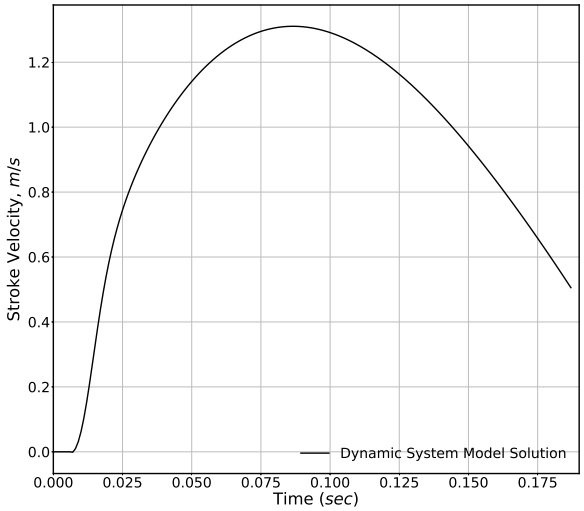


Figure 2: Shock absorber stroke velocity profile from a dynamic system model simulating a drop test, which is used to choose a suitable inlet velocity value in the LES study.

The flow in the present simulation is assumed to be incompressible, which is justified due to the low Mach number prevalent throughout the computational domain, and, since the focus of the study is on the free shear layer under a constant inlet velocity, we ignore the influence of the transient compression pressure waves associated with the movement of the piston in a real shock absorber. This assumption helps to increase the efficiency of the simulation by allowing the numerical stability to be determined by the hydrodynamic time-scale rather than the more restrictive acoustic time-scale.

The edge of the free shear layer for each profile was found locally based on the vorticity magnitude and streamwise velocity value, and then the high and low velocity values across the profile were defined, and their difference was used for normalisation of the velocity values across that specific profile. The self-similarity distance variable η is defined according to Equation (1) where the capital vertical coordinate Y has its origin at the orifice exit.

$$\eta = \frac{x - D_{orifice}/2}{Y}, \tag{1}$$

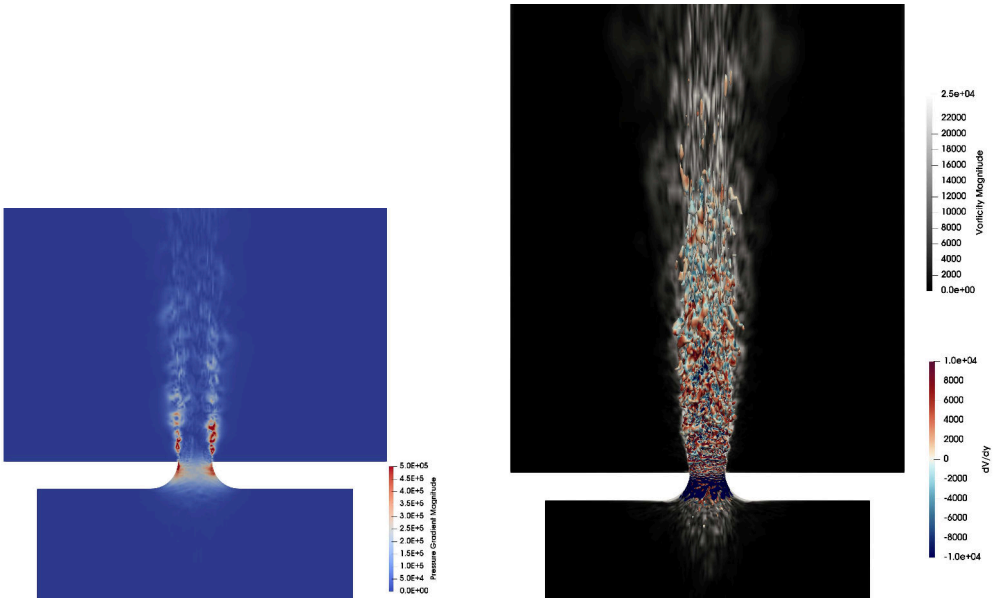
It should be noted that, in the present simulation, the streamwise direction is along the vertical y-direction with the corresponding velocity component and turbulent (Reynolds) stress component, $\overline{v'v'}$. For the purposes of analysing the near-field free shear layer development, a two-dimensional (2D) section (x-y plane at $z = 0$) is extracted from the three-dimensional

domain, where the mixing layer is quasi two-dimensional within a distance equivalent to a few orifice diameters downstream of the orifice exit.

In this region, the mixing layer is expected to exhibit standard behaviour that can be used to validate the simulation against similar mixing layer characteristics reported in experiments, which is a substitute for the lack of internal shock absorber data available in the literature. Noting that the Cylindrical and Cartesian coordinate systems are equivalent on the extracted x–y plane, the cross-flow Reynolds stress component is $\overline{u'u'}$, and the spanwise stress component is $\overline{w'w'}$ relative to the mixing layer development in the quasi two-dimensional region.

4 RESULTS AND DISCUSSION

4.1 SINGLE PHASE TURBULENT SHEAR LAYER



(a) Pressure gradient contours

(b) Q Criterion iso-surfaces superposed on vorticity magnitude contours

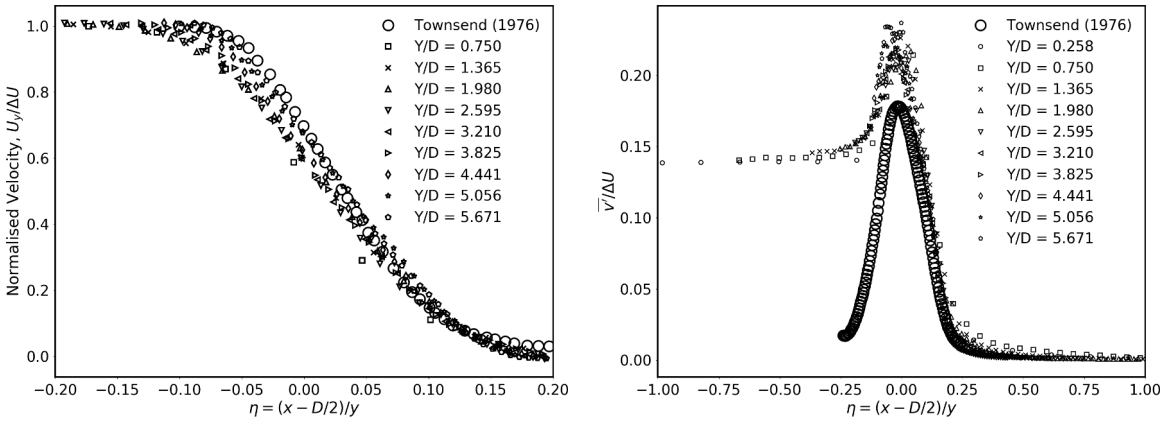
Figure 3: Flow development in the vicinity of the orifice

Turbulence can be visualised using the Q-criterion, which is found by plotting the iso-surfaces of the second invariant of the velocity strain rate tensor as shown in Fig. 3. The gradual development of increasingly complex flow structures in the shear layer is observed as initially quasi two-dimensional instabilities, such as ring vortices in Fig. 3b, develop into more complex structures and breakdown to smaller scales, until the full turbulent cascade is established further downstream of the orifice.

The Q iso-surfaces in Fig. 3b are plotted over vorticity magnitude contours to visualise the regions where flow unsteadiness is detected. The high vorticity magnitude values in the turbulent shear layers downstream of the orifice are expected as a consequence of the turbulent

flow in that region. However, it is also found that there is a region of significantly high vorticity magnitude upstream of the orifice. This is likely to be caused by the strong blockage effect of the orifice causing rapid flow direction change from the converging radially inward flow towards the axis of symmetry to streamwise flow through the orifice.

Pressure gradient contours in Fig. 3a are used to identify regions of high static pressure variation, which can be indicative of regions on the converging orifice surface susceptible to the formation of cavitation bubbles. These regions of relatively high cavitation formation potential will be revisited in the multiphase simulation section, where the results are consistent with the findings here.



(a) Streamwise velocity

(b) Streamwise turbulent stress

Figure 4: Free shear layer self-similarity

Another important observation is the tendency of mixing layers towards an approximately self-similar state, while moving in the streamwise direction [11]. This state is reached once the free shear layer passes the initial transitional stage near the tip and enters the turbulent regime around one orifice diameter downstream of the exit, where the profiles of turbulent flow variables taken across the shear layer tend to collapse onto a single profile once they are normalised appropriately.

The velocity profiles are plotted in Fig. 4a, in which the tendency towards a self similar profile is clearly manifested. It is seen in Fig. 4 that the first profile plotted at $Y/D_{orifice} = 0.75$ exhibits a more visible deviation from the self-similar profile, which is not surprising given that the turbulence flow is still developing at this location, as seen in the visualisation in Fig. 3. The profiles downstream become increasingly more conforming to the self-similar profile. Other turbulent properties are also expected to exhibit self-similarity. Profiles of the cross flow Root Mean Squared (RMS) component $\sqrt{\overline{u'u'}}$ are also plotted in Fig. 4b, where it is again demonstrated that the normalised profiles tend to collapse towards a single curve on moving downstream.

The stress profiles require a longer streamwise distance to reach approximate self-similarity when compared with the velocity profiles. This observation is consistent with the findings of

previous mixing layer investigations. However, the less common observation, in the context of a standard mixing layer, is that the RMS profiles in Fig. 4b seem to have a higher value on the negative η side, corresponding to the flow on the high velocity (jet) side of the free shear layer. This observed flow unsteadiness upstream of the orifice is further explored in Sheikh Al-Shabab *et. al.* [9], and it is consistent with the upstream unsteadiness visualised in Fig. 3b.

4.2 MULTIPHASE SIMULATION

Multiphase simulations are conducted on an unstructured two-dimensional axisymmetric domain, where the layout and mesh are shown in Fig. 5, with an unsteady velocity inlet profile corresponding to the piston stroke velocity given in Fig. 2. The geometry used in these simulations, Fig. 1a, is simplified from the original to focus on the main multiphase interaction of interest, while reducing the geometrical complexity of orifice support tubes, cylinder telescoping bearings and snubber chamber details. Particularly since the details of these features are not readily available from the available documentation. The simulations are validated using the experimental data of Milwitzky and Cook [6].

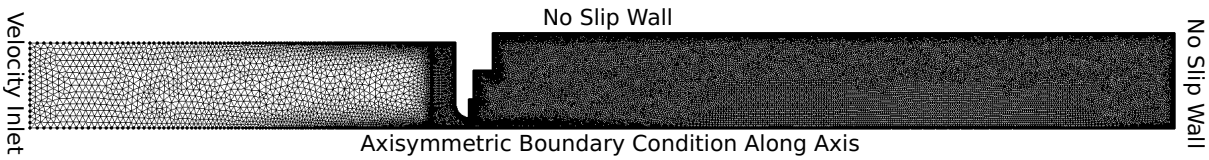
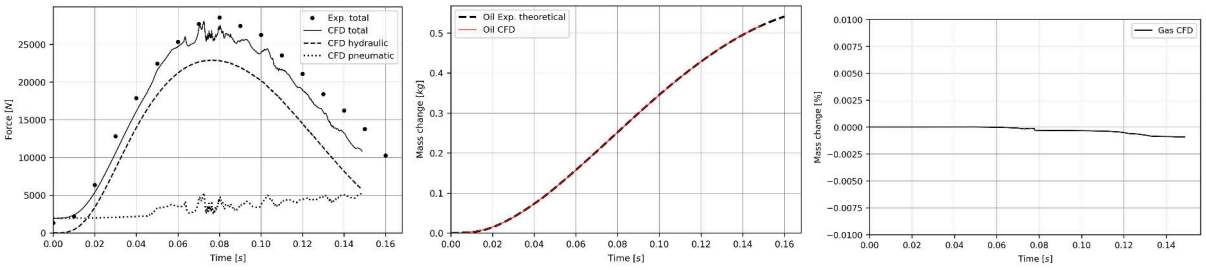


Figure 5: Simplified oleo pneumatic shock absorber 2D half domain mesh for validation case of Milwitzky and Cook [6]



(a) Force validation plot

(b) Oil mass change compared to calculated mass change from experimental data

(c) Gas mass variation in time

Figure 6: High-fidelity multiphase drop test case validation and report plots

The validation of the drop test case was performed against the available experimental data, which consists of the measured total force exerted by the shock absorber in the time span from impact at $0.0s$ to $0.16s$. The comparison plot of experimental measurements with CFD data plotted on Fig. 6a demonstrates good agreement between the two, capturing the overall

trends and values relatively well. Individually, simulated hydraulic and pneumatic forces cannot be compared to experimental data, but their shape and growth provide additional confidence in the results. The pneumatic force plot follows the shape of the theoretical pressure growth expected of an ideal gas. Pressure measurements for this plot were taken as averaged pressure over the top wall of the shock absorber, giving the sudden jumps in pneumatic force plot at certain times. These values are taken from this position to account for the fact that pressure propagation and distribution in the upper chamber is not uniform, and the measurements taken at top wall correspond to pneumatic force contribution to total force felt by the measuring equipment in the experiment. Hydraulic force, on the other hand, cannot be directly measured from CFD simulations and is calculated using:

$$F_h = \rho \frac{A_h^3}{2C_D^2 A_0^2} \dot{s}|\dot{s}|, \tag{2}$$

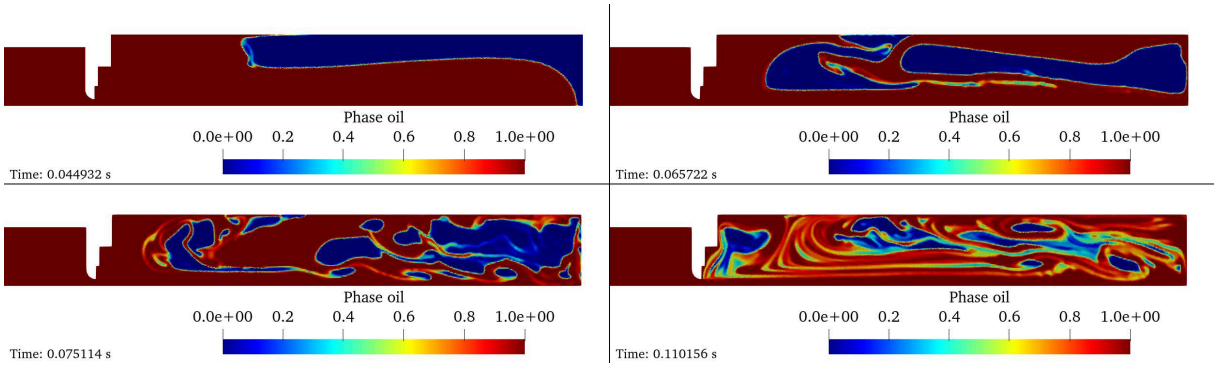
where A_h is the hydraulic area, C_D is the discharge coefficient, A_0 is the orifice area, and $|\dot{s}|$ is the stroke rate or inlet velocity in the case of the static mesh in the present simulation. This formula shows that the total force is highly dependant on the stroke rate, which is also demonstrated through shape similarity between the hydraulic force curve in Fig. 6a and the shape of the inlet velocity curve shown in Fig. 2. Additionally, discharge coefficient C_D is an important influential parameter in the hydraulic force calculation, given by:

$$C_D = \frac{Q_{experimental}}{Q_{theoretical}} = \frac{\dot{m}}{\rho A_0 u_{max}}, \tag{3}$$

where $\dot{m}$ is the mass flow through the orifice, and u_{max} is the maximum velocity downstream of the orifice, at the point of venna contracta. The maximum velocity is taken as maximum value from ten probes placed downstream of the orifice because the position of venna contracta depends on fluid velocity through the orifice. Hydraulic force and discharge coefficient calculation accuracy is not beneficial only to high-fidelity simulations, as it could also be utilised to improve the accuracy of low-fidelity model predictions. Through Equation 2 above, the discharge coefficient can be directly linked to stroke rate, and geometric features such as orifice shape, and the ratio of upper chamber to orifice cross sectional area.

Further validation of high-fidelity multiphase simulation was performed by monitoring the mass conservation of each phase in the upper chamber. The resulting plots are shown on Figs. 6b and 6c. The mass change of each phase from CFD simulations has been exported directly and plotted. Gas is not added or removed from the upper chamber so the validating plot in Fig. 6c shows its variation in time, which ideally should be equal to zero at all times. Some minor variation is present but it is below 0.001 % of total gas mass, which is small enough to be considered insignificant. The oil mass change is compared to mass change calculated from available experimental data. Knowing the stroke rate and lower chamber diameter, it is possible to calculate the volumetric inflow into the upper chamber. When compared with oil mass change directly exported from CFD simulations, the two show near perfect agreement in Fig. 6b.

The contours of flow field variables taken at four focused time steps are shown in Fig. 7 to demonstrate flow development. The progression and severity of phase mixing throughout the



(a) Phase contour plot

Figure 7: High-fidelity multiphase drop test case contour plots

simulation are illustrated with phase contour plots in Fig. 7a. The simulated drop down impact on the shock absorber causes a jet of oil to rise through the orifice axis and hit the top wall, redirecting the oil flow along the domain walls, creating a large recirculation region extending along the upper chamber. The phase mixing starts as the oil loops along the side wall, splitting the gas bubble into two main bubbles. Part of the gas sinks down towards the orifice and impacts the oil jet, causing the gas bubble to breakdown and disperse further as parts of it get convected with the jet. The other gas bubble from the initial gas breakup is pushed into the *dead fluid* recirculation zone in the bottom corner of the upper chamber. As the simulation progresses, this bubble stays in the recirculation zone and feeds gas into the oil jet as it leaves the orifice. The two phases mix extensively as these processes occur.

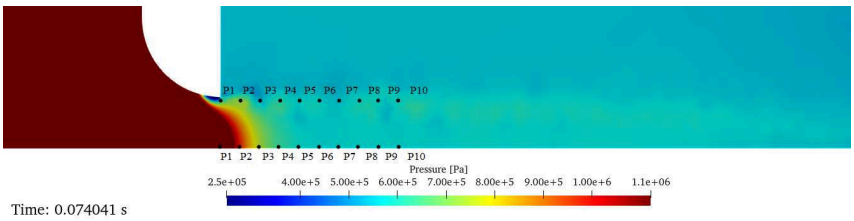


Figure 8: Multiphase drop test simulation – pressure field around the orifice with placed pressure probes

A region of interest for cavitation occurrence is around the tip of the orifice. The low pressure region, identified in the pressure contour plot in Fig. 8 focusing on the orifice tip and area around it, indicates the possibility of cavitation inception there. Although cavitation modelling is not included in this simulation, the potential for its occurrence is monitored with pressure probes distributed in regions of interest. The figure shows ten probes on the axis of symmetry, and ten probes along the orifice tip placed in the downstream direction. The coordinate system origin is placed at the point of symmetry line coinciding with the orifice exit plane. The probes are uniformly distributed in the downstream direction between $x = 0m$ and $x = 0.018m$, so that the horizontal separation between two adjacent probes is $\delta x = 0.002m$.

4.3 MULTIFIDELITY FRAMEWORK

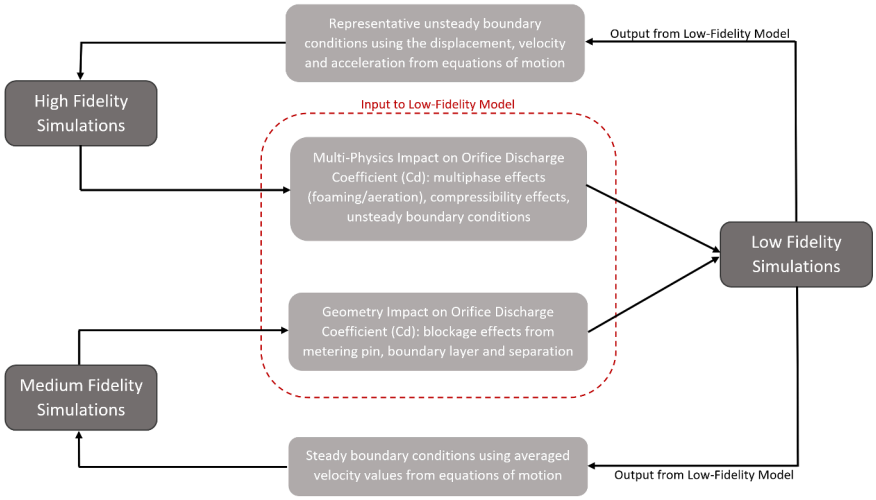


Figure 9: Multi-Fidelity interaction to refine discharge coefficient estimate and provide boundary conditions

The estimation of the orifice discharge coefficient provides a useful demonstration of the likely interaction between the different fidelity levels, as shown in Fig 9. The low-fidelity solution of the dynamic system equations of motion can provide case specific values for the relative piston displacement, velocity and acceleration at user specified time intervals that can be used as boundary conditions for moving parts in high-fidelity simulations. Alternatively, the velocity values could be averaged or taken at a stroke value of interest and used as a steady state boundary condition in medium-fidelity simulations. In both cases, the low-fidelity solution can be used to provide more accurate case specific boundary condition for the higher fidelity simulations. On the other side, high fidelity results can be used to improve the low-fidelity parameter values, such as the discharge coefficient, over the various stages of the stroke.

5 CONCLUSIONS

The simulation of oleo-pneumatic shock absorber internal dynamics was discussed. The numerical requirements for the different aspects of the flow physics were found to make a modular approach more efficient in tackling the multiphysics nature of the shock absorber flow field. Single phase three dimensional scale resolving simulations were conducted to focus on the shear layer development downstream of the orifice. In addition, multiphase two dimensional axisymmetric simulations were used to investigate the interaction and mixing between the gas and oil in the shock absorber. The simulations were validated against a drop down experiment and some standard physical results. A low fidelity approach, based on a dynamic systems model of the shock absorber, was used to provide quick return simulations to explore the design space and

provide case specific boundary conditions for the higher fidelity simulations. A multi-fidelity approach that utilises these different methods can then be adopted to fine tune the low fidelity solver, to populate the design space and to investigate the impact of variations in some key design parameters.

6 Acknowledgements

This research was funded by Innovate UK grant number 263261 and Airbus Operations Ltd. The underlying data can be accessed using the DOI: 10.17862/cranfield.rd.20060153.

REFERENCES

[1] P. Bradshaw, D. H. Ferriss, and R. Johnson. Turbulence in the noise-producing region of a circular jet. *Journal of Fluid Mechanics*, 19(4):591–624, 1964.

[2] N. Currey. *Aircraft Landing Gear Design: Principles and Practices*. AIAA education series. American Institute of Aeronautics and Astronautics, 1988.

[3] T. Holzmann. Mathematics, numerics, derivations and openfoam®. *Loeben, Germany: Holzmann CFD*, 2016.

[4] R. Issa. Solution of the implicitly discretised fluid flow equations by operator-splitting. *Journal of Computational Physics*, 62(1):40–65, 1986.

[5] H. Jasak. *Error analysis and estimation for the finite volume method with applications to fluid flows*. PhD thesis, Imperial College London, 1996.

[6] B. Milwitzky and F. E. Cook. Analysis of landing-gear behavior. *NACA Technical Note*, (TN-2755), 1952.

[7] F. Nicoud and F. Ducros. Subgrid-scale stress modelling based on the square of the velocity gradient tensor. *Flow, turbulence and Combustion*, 62(3):183–200, 1999.

[8] S. Patankar and D. Spalding. A calculation procedure for heat, mass and momentum transfer in three-dimensional parabolic flows. *International Journal of Heat and Mass Transfer*, 15(10):1787–1806, 1972.

[9] A. A. Sheikh Al-Shabab, B. Grenko, D. Vitlaris, P. Tsoutsanis, A. F. Antoniadis, and M. Skote. Numerical investigation of orifice nearfield flow development in oleo-pneumatic shock absorbers. *Fluids*, 7(2), 2022.

[10] A. A. Sheikh Al-Shabab, D. Vitlaris, Z. Lin, B. Grenko, P. Tsoutsanis, A. F. Antoniadis, and M. Skote. Numerical investigation of oleo-pneumatic shock absorber: Setup and validation. *WCCM-ECCOMAS2020*.

[11] A. Townsend. *The structure of turbulent shear flow*. Cambridge university press, 1980.

[12] H. G. Weller, G. Tabor, H. Jasak, and C. Fureby. A tensorial approach to computational continuum mechanics using object-oriented techniques. *Computers in physics*, 12(6):620–631, 1998.



https://dspace.org/

Numerical investigation of oleo-pneumatic shock absorber: a multi-fidelity approach

Sheikh Al Shabab, Ahmed; Grenko, Bojan; Vitlaris, Dimitrios; Tsoutsanis, Panagiotis; Antoniadis, Antonis ...

2022-11-24
ECCOMAS
https://doi.org/10.23967/eccomas.2022.201
Sheikh Al-Shabab AA, Grenko B, Vitlaris D, et al., (2022) Numerical investigation of oleo-pneumatic shock absorber: a multi-fidelity approach. In: ECCOMAS Congress 2022 - 8th European Congress on Computational Methods in Applied Sciences and Engineering, 5-9 June 2022, Oslo, Norway

Downloaded from a DSpace repository. https://dspace.org/